

Research Paper

Repurposing Ponatinib as a Potent Agent against *KIT* Mutant Melanomas

Yong Han^{1,2,3*}, Ziyue Gu^{1,2,3*}, Jing Wu^{1,2,3*}, Xiaojuan Huang^{1,2,3}, Rong Zhou^{1,2,3}, Chaoji Shi², Wenjie Tao^{1,2,3}, Lizhen Wang⁴, Yanan Wang¹, Guoyu Zhou¹, Jiang Li⁴, Zhiyuan Zhang^{1,2,3}✉, Shuyang Sun^{1,2,3}✉

1. Department of Oral and Maxillofacial-Head & Neck Oncology, Ninth People's Hospital, Shanghai Jiao Tong University School of Medicine, Shanghai 200011, P.R. China.
2. National Clinical Research Center for Oral Diseases, Shanghai 200011, P.R. China.
3. Shanghai Key Laboratory of Stomatology & Shanghai Research Institute of Stomatology, Shanghai 200011, P.R. China.
4. Department of Oral Pathology, Ninth People's Hospital, Shanghai Jiao Tong University, School of Medicine, Shanghai 200011, P.R. China.

*These authors contributed equally to this work.

✉ Corresponding authors: shuyangs@shsmu.edu.cn and zhzy@sjtu.edu.cn

© Ivyspring International Publisher. This is an open access article distributed under the terms of the Creative Commons Attribution (CC BY-NC) license (<https://creativecommons.org/licenses/by-nc/4.0/>). See <http://ivyspring.com/terms> for full terms and conditions.

Received: 2018.10.23; Accepted: 2019.01.22; Published: 2019.03.16

Abstract

Rationale: Mutations in *KIT*, a major cancer driver gene, are now considered as important drug targets for the treatment of melanomas arising from mucosal and acral tissues and from chronically sun-damaged sites. At present, imatinib is the only targeted drug for *KIT*-mutation-bearing melanomas that is recommended by the National Comprehensive Cancer Network (NCCN) Clinical Practice guidelines. Patients with *KIT* mutations, however, are either insensitive or rapidly progress to imatinib insensitivity, which restricts its clinical use. Thus, effective inhibitors of *KIT*-mutation-bearing melanomas are urgently needed.

Methods: A cohort of patient-derived tumor xenograft (PDX) models and corresponding PDX-derived cells (PDCs) from patients with melanomas harboring *KIT* mutations (*KIT*^{V560D}, *KIT*^{K642E} and *KIT*^{D816V}) were established, characterized, and then used to test the *in vitro* and, subsequently, *in vivo* inhibitory effects of a panel of known *KIT* inhibitors.

Results: Ponatinib was more potent than imatinib against cells bearing *KIT* mutations. *In vivo* drug efficacy evaluation experiments showed that ponatinib treatment caused much stronger inhibition of *KIT*-mutation-bearing melanomas than did imatinib. Mechanistically, molecular dynamics (MD) simulations revealed a plausible atomic-level explanation for the observation that ponatinib has a higher affinity for the *KIT*^{D816V} mutant protein than does imatinib.

Conclusions: Our study of *KIT*-mutation-and *KIT*^{WT}-bearing melanomas demonstrates that ponatinib is a far more potent inhibitor than is imatinib for *KIT*-mutation-bearing melanomas and thus underscores that ponatinib should be given priority consideration for the design of precision treatments for melanoma patients triaged to have *KIT* mutations. Moreover, our work provides a rationale for undertaking clinical trials to examine the repurposing of ponatinib, which is already approved for use in leukemia, for use in treating a large subset of melanoma patients.

Key words: ponatinib, melanomas, *KIT*, patient-derived xenograft models

Introduction

Melanomas are tumors that arise from melanocytes located in a large variety of anatomic sites. The incidence of melanoma is rising steadily worldwide; it has increased nearly fourfold in the past 30 years [1]. Fortunately, as recent insights from oncobiological

research have identified some of the driver genes for many cancers, melanoma patients now can be clinically stratified based on the molecular characteristics of their tumors [2], and some of these patients have benefited enormously from significant

clinical breakthroughs in precision medicine (e.g., vemurafenib treatment has been successfully applied in patients harboring the *BRAF*^{V600E/V600K} mutation) [3]. Certain melanomas, particularly those arising from mucosal and acral tissues and chronically sun-damaged sites, frequently feature oncogenic mutations in the *KIT* gene [4]. *KIT* mutations induce ligand-independent receptor activation, which constitutively activates a series of downstream pathways, including the MAPK and PI3K-mTOR signaling cascades [5]; *KIT* is thus now viewed as a critically vulnerable target for the treatment of melanomas.

Imatinib, a multikinase inhibitor of *KIT*, *ABL*, and *PDGFR* [6], is currently the only targeted drug for *KIT*-mutant melanomas recommended in the Clinical Practice Guidelines of the National Comprehensive Cancer Network. However, it is now well documented that the efficacy of imatinib in treating melanomas varies greatly depending on the presence of the particular type of *KIT* mutation sites in a given tumor, and the therapeutic effect of imatinib is apparently limited to *KIT* mutations located on exons 11 and 13 but not exon 17 [7]. Specifically, clinical trials have indicated that the average time to disease progression after imatinib treatment for patients bearing *KIT*-associated (mutation or copy number amplification) tumors is approximately 3–4 months [8–10].

Notably, several alternative *KIT* inhibitors have been evaluated for use in treating *KIT*-mutation-bearing melanomas that are resistant to imatinib, including sunitinib [11], dasatinib [12], and nilotinib [13]. However, with each of these three compounds, despite the fact that early disease control was achieved, their efficacy was still modest, and the cancers of most patients in the studies ultimately progressed. Given the limited clinical benefits of these drugs and considering that between 7.6% and 47% of melanomas harbor *KIT* mutations (varying by subtype) [14–16], new therapies for patients with *KIT*-mutant melanomas are critically needed.

Patient-derived tumor xenograft (PDX) models are powerful preclinical experimental tools that can retain the histological and genetic characteristic of patient tumors to a large extent [17]. PDX models can faithfully and characteristically respond to targeted therapies and are now popularly used in preclinical drug testing [18]. Indeed, many recent studies have underscored the suitability of using PDX models as precision medicine platforms for drug screening, biomarker discovery, and the development of other personalized medicine strategies [19, 20].

Here, in light of the poor efficacy of imatinib in treating *KIT*-mutation-bearing melanomas, and with the goal of identifying effective *KIT* inhibitors to provide alternative therapeutic options for *KIT*

mutant melanoma patients, we developed a series of *KIT*-mutant PDX models from melanoma patients and used these models to evaluate the antitumor efficacy of a variety of known *KIT* inhibitor compounds. This examination of drug efficacy, first via screening in cells and then a successive *in vivo* validation in our genetically characterized PDX models, revealed that ponatinib, an FDA-approved chronic myeloid leukemia (CML) drug, was the most potent inhibitor of tumor growth of against *KIT*-mutation-bearing melanomas. Furthermore, immunoblotting with phosphorylation-specific antibodies confirmed that, both *in vitro* and *in vivo*, ponatinib-induced inhibition of *KIT* reduced the extent of phosphorylation of its downstream signaling targets. Finally, our molecular dynamics simulations suggested that the significantly improved inhibitory activity of ponatinib compared with imatinib can be attributed to its stronger binding affinity to mutated *KIT* proteins. Our study demonstrated that ponatinib is a potent agent against *KIT*-mutation-bearing melanomas and underscored how the repurposing of drugs can help develop effective precision treatments for a substantial proportion of melanomas that are insensitive to the drugs that are currently recommended by NCCN guidelines.

Results

Establishing PDX models of *KIT*-mutation-bearing melanomas and screening of kinase inhibitors for antitumor efficacy

Seeking to establish an experimental platform to explore possible alternative treatments for imatinib-resistant melanomas, we identified mucosal melanoma patients, each with a different *KIT* mutation (*KIT*^{V560D}, *KIT*^{K642E}, *KIT*^{D816V}), as well as a non-*KIT* mutation melanoma patient, and generated PDX models from each patient (Figure 1A). The similarity of the established PDX models with the corresponding patient samples was validated using DNA sequencing, HE staining, and immunostaining against the melanoma markers HMB-45 and Melan-A and the cell growth marker Ki-67 (Figure 1B and Figure S1A and Figure S2A). Previous studies have reported that two of these *KIT* mutations (*KIT*^{V560D}, *KIT*^{K642E}) are highly sensitive to imatinib treatment and that *KIT*^{D816V} is completely insensitive to imatinib [8–10, 21]. Unexpectedly, when we treated the reportedly imatinib-sensitive *KIT*^{V560D} and *KIT*^{K642E} mutations in PDX models with imatinib, we did not find a significant difference in tumor growth inhibition (TGI) between the imatinib (100 mg/kg) and the control groups (Figure 2A–D, PDX-*KIT*^{V560D}, TGI =

35.81%, $P > 0.05$; PDX- KIT^{K642E} , TGI = 25.58%, $P > 0.05$). This surprising result is not in accord with previous results on the sensitivity of these mutations to imatinib and thus suggests that more research will be needed to develop more potent drugs for these patients.

Next, we isolated primary tumor cells from the established KIT mutant PDX models for *in vitro* inhibition assays (Figure 1C and Figure S1B and Figure S2B); we conducted drug dose-response assays of these cells for a series of clinically evaluated kinase inhibitors with reported activity against KIT , including axitinib, dasatinib, nilotinib, ponatinib, sorafenib and sunitinib. The PDX- KIT^{WT} -derived cells had poor responses to all of these inhibitors (Figure 3A). These assays revealed that ponatinib, an

FDA-approved drug for the treatment of CML, was more potent than was imatinib against the PDX-derived cell (PDC)- KIT^{V560D} , with an IC_{50} value of 39.05 nM versus 75.66 nM for imatinib (Figure 3B and Table S1). For the PDC- KIT^{V560D} , dasatinib and axitinib were also more effective than was imatinib, with IC_{50} values of 34.59 nM and 23.98 nM, respectively; nilotinib and sorafenib showed poor inhibition effects against PDC- KIT^{V560D} (Table S1). Similar results were observed in the PDC with the KIT^{K642E} mutation (Figure 3C and Table S1). For the PDC harboring the reportedly imatinib-resistant KIT^{D816V} mutation, imatinib induced very little inhibition (IC_{50} value of 4840 nM), but ponatinib exhibited the highest inhibitory effect (IC_{50} value of 174.3 nM, Figure 3D and Table S1).

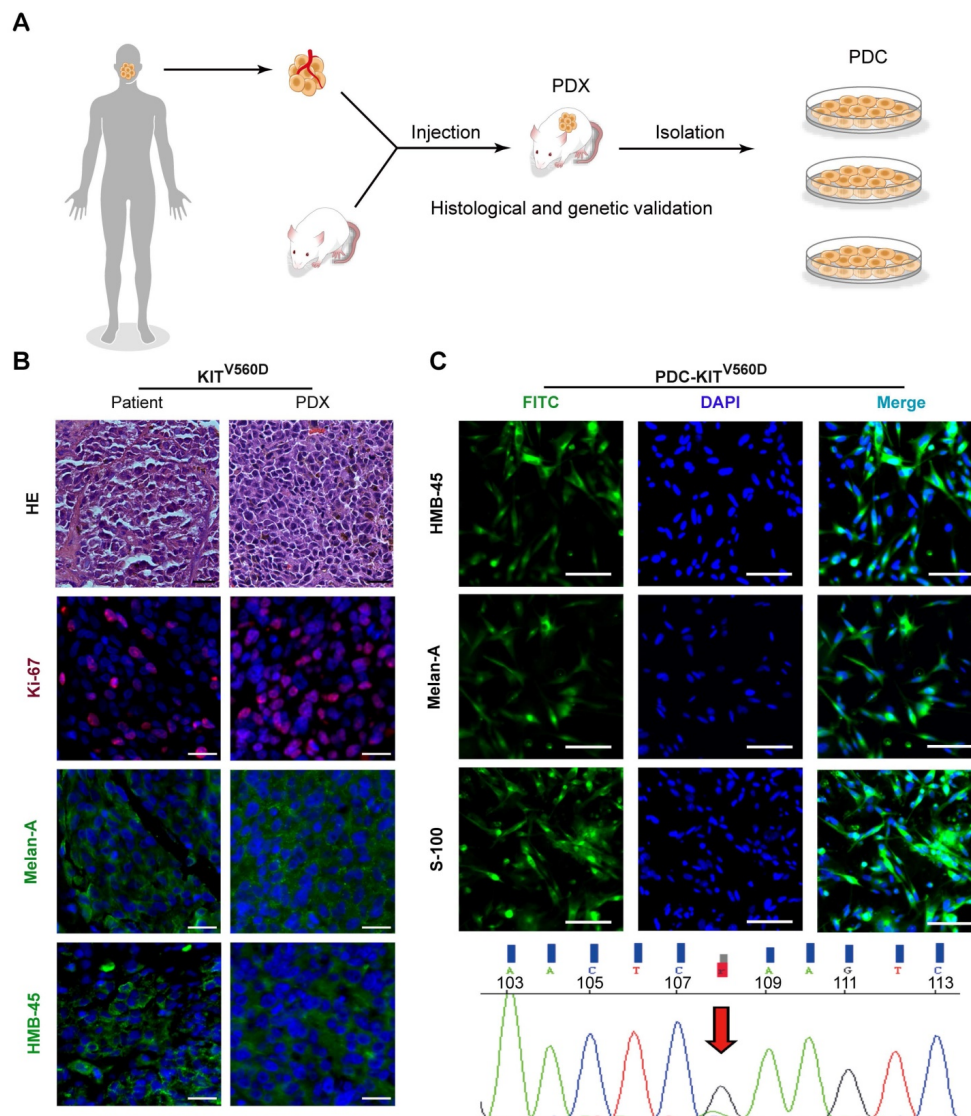


Figure 1. Establishment and characterization of KIT^{V560D} PDX models. **(A)** Schematic of PDX and PDC establishment. **(B)** Representative hematoxylin and eosin (H&E) staining and immunofluorescence staining of patient tumors and corresponding PDX model tumors. HMB-45 and Melan-A (both green), Ki-67 (red) and DAPI (blue). The scale bar is 100 μ m. **(C)** Representative immunofluorescence staining of patient-derived tumor cells from KIT^{V560D} mutant melanoma PDX models are shown in the upper panel, and the KIT mutation status of the corresponding PDX-derived cells is shown in the bottom panel. HMB-45, Melan-A and S-100 (both green), and DAPI (blue). The scale bar is 100 μ m.

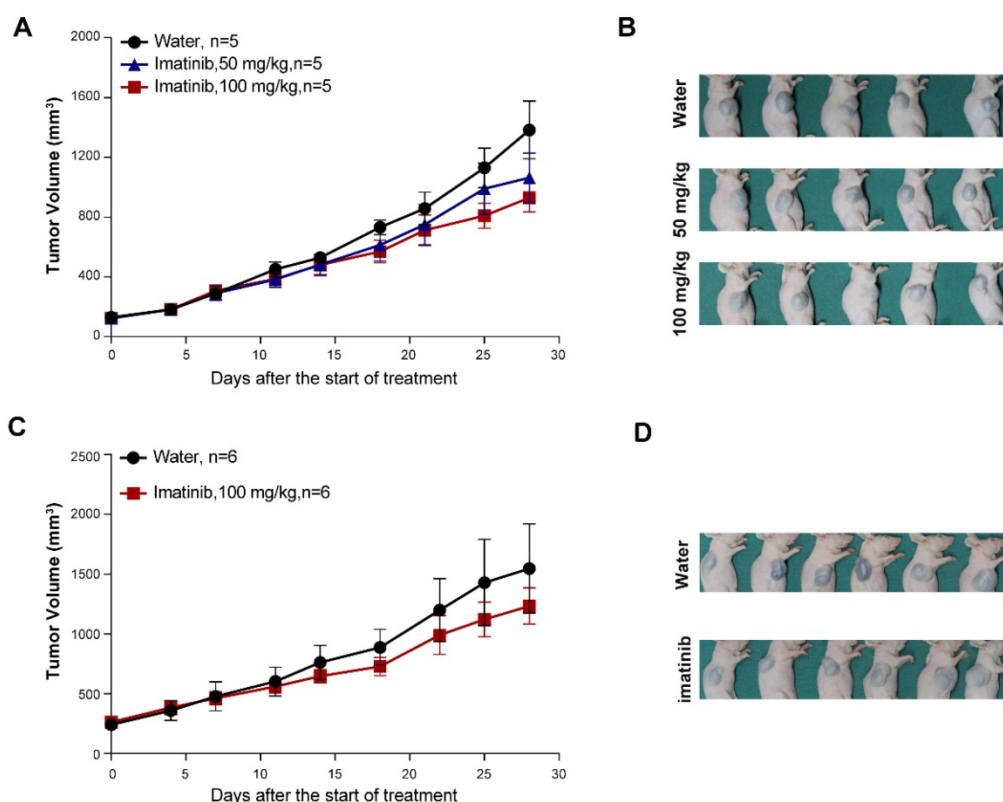


Figure 2. *In vivo* evaluation of imatinib efficacy in *KIT*^{V560D} and *KIT*^{K642E} mutant PDX models. **(A-B)** Inhibition efficacy of imatinib in PDX models with *KIT*^{V560D} mutation (n= 5 mice per group). Imatinib, 50 mg/kg, tumor growth inhibition, TGI= 25.04%, $P > 0.05$; imatinib, 100 mg/kg, TGI= 35.81%, $P > 0.05$, Student's *t*-test. **(C-D)** Inhibition efficacy of imatinib in PDX models with *KIT*^{K642E} mutation (n=6 mice per group). Imatinib, 100 mg/kg, TGI = 35.81%, Student's *t*-test, $P > 0.05$.

We also compared the inhibitory effect of imatinib and ponatinib on serial *KIT*-dependent Ba/F3 cells, including *KIT*^{WT}, *KIT*^{V560D}, *KIT*^{K642E} and *KIT*^{D816V} mutations. Consistent with the results in PDCs, ponatinib demonstrated a higher potency for *KIT*^{V560D}, *KIT*^{K642E} and *KIT*^{D816V} in Ba/F3 cells than did imatinib (**Figure S3 and Table S2**). Notably, all the IC₅₀s of ponatinib in these *KIT*-dependent Ba/F3 cells were lower than that of dasatinib, indicating ponatinib could also exerted greater inhibitory effect when compared with dasatinib (**Figure S3 and Table S2**).

To confirm that the observed decreases in cell viability resulted from specific inhibition of *KIT* signaling, we conducted immunoblotting assays to test the phosphorylation status of *KIT* and its downstream signaling targets in the PDCs after 2 hours of treatment with imatinib, ponatinib, or dasatinib. Consistent with the cell viability results, ponatinib and dasatinib reduced the phosphorylation levels of *KIT*, *AKT*, and *ERK* in a dose-dependent manner, whereas imatinib did not strongly affect the phosphorylation levels of these downstream *KIT* target proteins (**Figure 3E-H**).

***In vivo* evaluation of ponatinib efficacy**

PDX models are now popular *in vivo* models for

drug evaluation. We conducted a preclinical evaluation based on our genetically characterized melanoma PDX models to validate the drug efficacies observed in our *in vitro* studies. Single-agent treatments were performed with imatinib (100 mg/kg), dasatinib (30 mg/kg) and ponatinib (30 mg/kg) in PDX models. Treatment of PDX-*KIT*^{WT} model with imatinib, ponatinib, or dasatinib did not cause significant differences in tumor growth (**Figure 4A-C and Table S3**). For the PDX-*KIT*^{V560D}, ponatinib (TGI=78.33%) exhibited the greatest tumor growth inhibition effects, and dasatinib (TGI=68.65%) had better inhibition efficacy than did imatinib (TGI=25.25%, **Figure 4D-F and Table S3**). Similarly, in PDX-*KIT*^{K642E}, both ponatinib (TGI=83.66%) and dasatinib (TGI=81.38%) exhibited more effective inhibition than did imatinib (TGI=27.59%, **Figure 4G-I and Table S3**). Strikingly, for the PDX-*KIT*^{D816V}, ponatinib (TGI=99.95%) displayed almost complete suppression of tumor growth, while dasatinib (TGI=67.73%) and imatinib (TGI=42.67%) showed much more modest effects (**Figure 4J-L and Table S3**). In addition, the drug toxicities of these inhibitors were all well tolerated during the preclinical trial (**Figure S4**).

To confirm that the observed TGI of the *KIT*-mutation-bearing melanomas was specifically due to the downregulation of *KIT* signaling, we measured

the phosphorylation levels of KIT, ERK, and AKT in the PDX tumors after 28 days of treatment. Treatment of the PDX-*KIT*^{WT} with ponatinib, dasatinib, and imatinib caused no significant difference in the levels of pKIT, pERK, or pAKT (Figure S5A). In contrast, treatment of the *KIT*-mutation-bearing PDX-*KIT*^{V560D}, PDX-*KIT*^{K642E} and PDX-*KIT*^{D816V} models with ponatinib and dasatinib significantly reduced the levels of pKIT, pERK, and pAKT, while imatinib showed only modest effects (Figure 5A and Figure S6A and Figure S7A).

We also used Ki-67 staining and TUNEL-assays to assess the proliferative and apoptotic status of the PDX tumors after 28 days of inhibitor treatment. Ponatinib treatment of PDX-*KIT*^{V560D}, PDX-*KIT*^{K642E} and PDX-*KIT*^{D816V} models resulted in a remarkable reduction in Ki-67-labeled cell proliferation and induced more TUNEL-labeled apoptotic cells than did imatinib, while no significant difference was observed for PDX-*KIT*^{WT} (Figure 5B-E and Figure S5B-E, Figure S6B-E and Figure S7B-E).

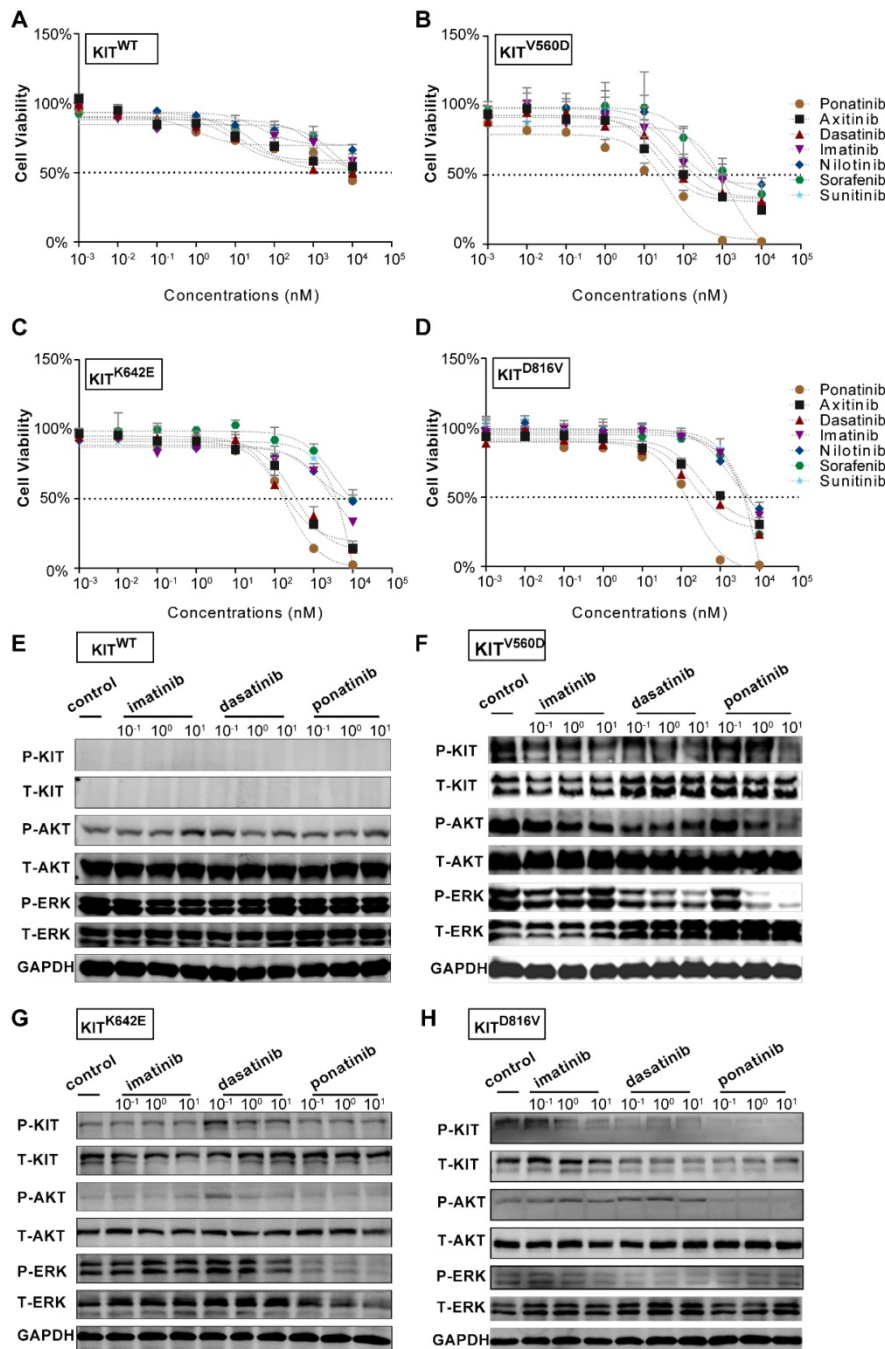


Figure 3. *In vitro* drug efficacy evaluation using *KIT*^{WT}, *KIT*^{V560D}, *KIT*^{K642E} and *KIT*^{D816V} PDX-derived cells. (A-D) Dose-response curve of imatinib, dasatinib, axitinib, nilotinib, ponatinib, sorafenib, and sunitinib in 72-h proliferation assays with *KIT*^{WT}, *KIT*^{V560D}, *KIT*^{K642E} and *KIT*^{D816V} PDX-derived cells. (E-H) Immunoblot analysis of *KIT* signaling in *KIT*^{WT}, *KIT*^{V560D}, *KIT*^{K642E} and *KIT*^{D816V} PDX-derived cells treated with imatinib, dasatinib, or ponatinib for 2 hours.

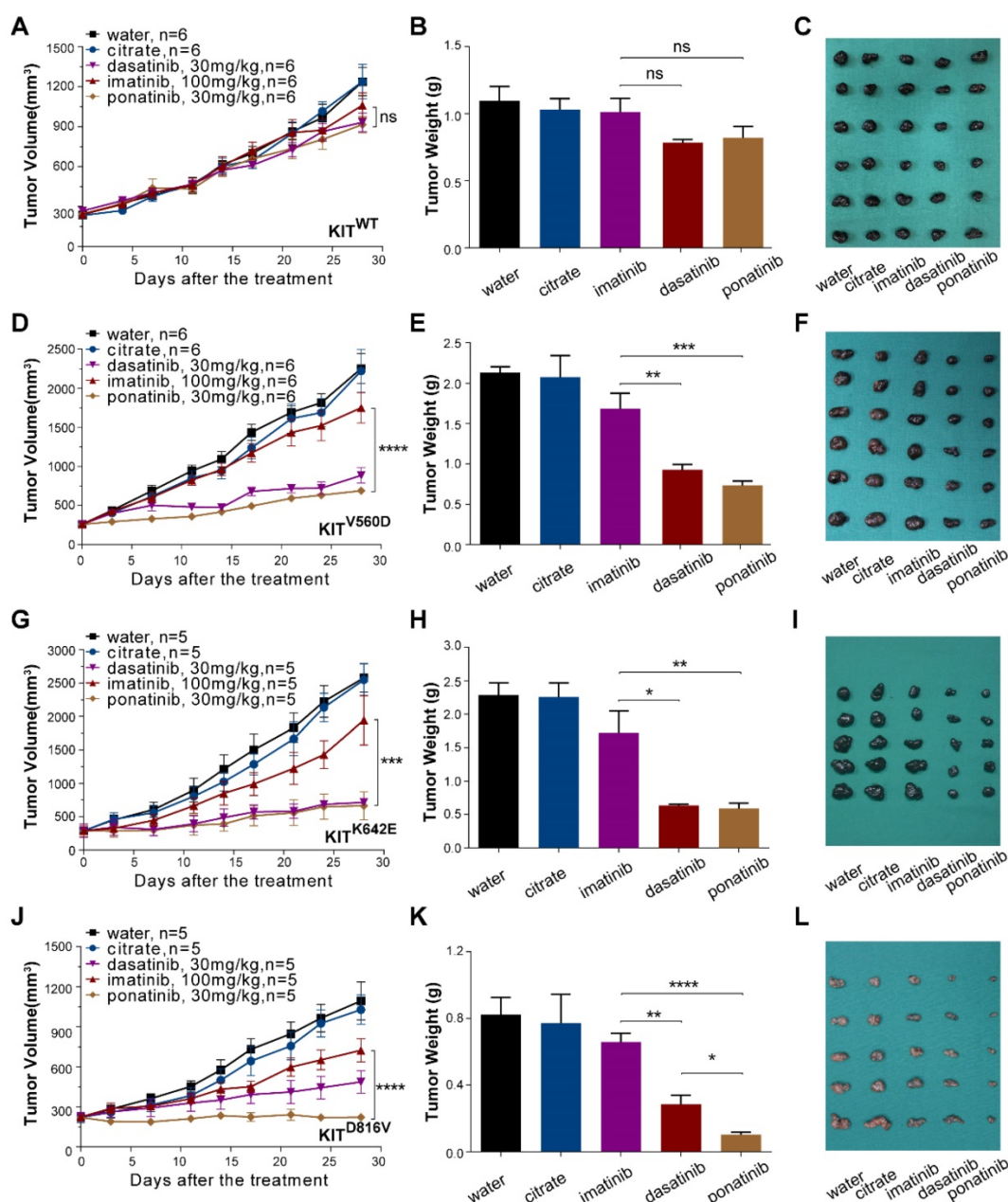


Figure 4. *In vivo* drug efficacy evaluation in *KIT*^{WT}, *KIT*^{V560D}, *KIT*^{K642E} and *KIT*^{D816V} mutant PDX models. We administered imatinib (100 mg/kg) and ponatinib (30 mg/kg) to PDX mice daily for 28 days. Tumor volume and tumor weight were measured, and the results are summarized as the mean \pm SEM (Student's *t*-test). Representative tumor images of these experiments (taken on day 28). **(A-C)** PDX-*KIT*^{WT}, treated with imatinib (TGI = 17.96%), dasatinib (TGI = 33.85%), and ponatinib (TGI = 33.26%), *n* = 6. **(D-F)** PDX with *KIT*^{V560D} mutation, treated with imatinib (TGI = 25.25%), dasatinib (TGI = 68.65%), and ponatinib (TGI = 78.33%), *n* = 6. **(G-I)** PDX with *KIT*^{K642E} mutation, treated with imatinib (TGI = 27.59%), dasatinib (TGI = 81.38%) and ponatinib (TGI = 83.66%), *n* = 5. **(J-L)** PDX with *KIT*^{D816V} mutation, treated with imatinib (TGI = 42.67%), dasatinib (TGI = 67.73%) and ponatinib (TGI = 99.95%), *n* = 5. * *P* < 0.05; ** *P* < 0.01; *** *P* < 0.001; **** *P* < 0.0001; ns, not significant; *n* indicates the number of tumors per arm.

To further explore the potential mechanisms of the inhibitory effects of ponatinib when compared with imatinib, we performed RNA-sequencing in *KIT*^{K642E} PDXs treated with imatinib (*n* = 3) and ponatinib (*n* = 3). A total of 1130 differential expressed genes were found in ponatinib-treated tumors when compared with imatinib-treated tumors, including 712 genes that were down-regulated and 418 genes that were up-regulated (Figure 6A). Kyoto Encyclopedia of Genes and Genomes (KEGG) enrichment

analysis was then performed on these differential expressed genes, and demonstrated that the extracellular matrix (ECM)-receptor interaction pathway was the most significantly downregulated pathway in ponatinib treated tumors (Figure 6B). Thus, these data indicated that downregulation of the ECM-receptor interaction pathway was a potential mechanism mediating the robust efficacy of ponatinib in tumor growth inhibition when compared with imatinib.

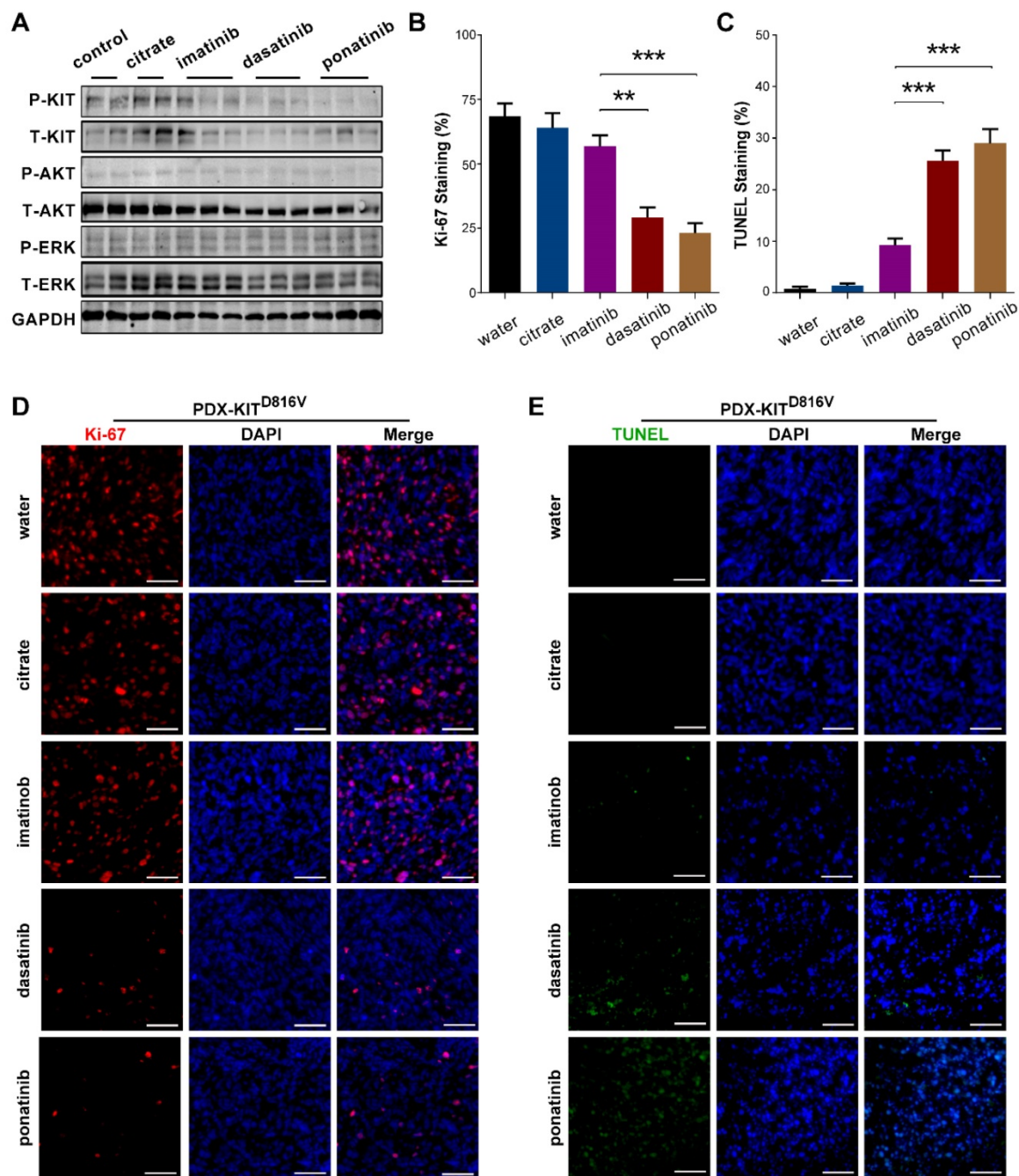


Figure 5. Inhibitory efficacy of ponatinib in PDX with *KIT*^{D816V} mutation. **(A)** Immunoblot analysis of *KIT* signaling in tumors after 28 days of treatment with imatinib, dasatinib and ponatinib. **(B)** Scoring of Ki-67 staining is summarized as the mean \pm SEM. Student's *t*-test, **, $P < 0.01$; ***, $P < 0.001$. **(C)** Scoring of TUNEL staining is summarized as the mean \pm SEM. Student's *t*-test, ***, $P < 0.001$. **(D)** Representative Ki-67 staining in tumors after 28 days treatment with imatinib, dasatinib and ponatinib. Scale bar, 50 μ m. **(E)** Representative TUNEL staining in tumors after 28 days of treatment with imatinib, dasatinib and ponatinib. Scale bar, 50 μ m.

Molecular dynamics simulations showing that ponatinib has a stronger affinity for *KIT*^{D816V} than imatinib

We used MD simulations to investigate the atomic basis of the observed dramatic difference in the inhibition efficacy of ponatinib versus imatinib for melanomas bearing *KIT* mutations. The crystal structure of ponatinib/imatinib-bound *KIT*^{WT} has been solved [22, 23]; but to date, there have been no studies

exploring whether *KIT* mutations specifically affect the affinity of ponatinib for the *KIT* protein. Considering that *KIT*^{D816V} is the most common imatinib-resistant mutation in melanomas [21], systemic mastocytosis [24] and several other malignancies [25], we selected *KIT*^{D816V} from among the *KIT* mutations and compared the binding dynamics using 100-ns MD simulations for four complexes: *KIT*^{WT}-imatinib, *KIT*^{WT}-ponatinib, *KIT*^{D816V}-imatinib, and *KIT*^{D816V}-ponatinib. To check for structural stability and to

assess the movements of the four complexes during the course of the simulation, the fluctuations of the KIT-inhibitor complex were analyzed by measuring root mean square deviation (RMSD) for the distance between the backbone atoms of the protein kinase domain and imatinib/ponatinib. After 40 ns, each of the four complexes reached a relatively stable state (**Figure 7A-B**), which indicated that these protein structures can be stably maintained in all four cases without a significant conformational change under the simulation conditions. Notably, the KIT^{D816V}-ponatinib complex had a lower RMSD value than did the KIT^{WT}-ponatinib complex, while there were no significant differences between the KIT^{D816V}-imatinib and KIT^{WT}-imatinib complexes. As imatinib and ponatinib exert their effect by blocking the ATP-binding site of the protein kinase, the result suggests that ponatinib was more constrained in the ATP-binding sites of KIT^{D816V} than was imatinib, leading to a relatively stronger affinity for KIT^{D816V} than did imatinib. As the mechanism of imatinib resistance to KIT^{D816V} has been investigated thoroughly using MD simulations, and the electrostatic interactions were considered to be a decisive factor affecting the binding energy, a significant decrease in

electrostatic interactions contributed to imatinib resistance to KIT^{D816V} [26]. We calculated the free binding energy in the ponatinib-KIT^{WT} and KIT^{D816V} complexes. Notably, the electrostatic energy (ΔG_{elect}) sharply increased in the ponatinib-KIT^{D816V} complex, while minor changes were observed in other binding energy components (**Table S4**), suggesting that the change in electrostatic interactions was the principle force contributing to the final binding energy (ΔG_{bind}). The salt bridge D792•••R815 is an important contributor to the electrostatic interaction between imatinib and KIT, and most importantly, it may contribute to the resistance of imatinib to KIT^{D816V} [26]. Next, we analyzed the salt bridge D792•••R815 in our inhibitor-KIT complexes. Significantly, divergent salt bridges were shown in the ponatinib-KIT^{D816V} complex but absent in the imatinib-KIT^{D816V} complex (**Figure S8A-B**). As D792 and R815 were charged residues located near the ATP-binding site, the salt bridge apparently changed the distribution of the charges of the residues in the region of the ATP-binding site, which was shown in the electrostatic potential (EP) surface of the imatinib-KIT^{D816V}-complex and the ponatinib-KIT^{D816V}-complex. (**Figure S8C-D**).

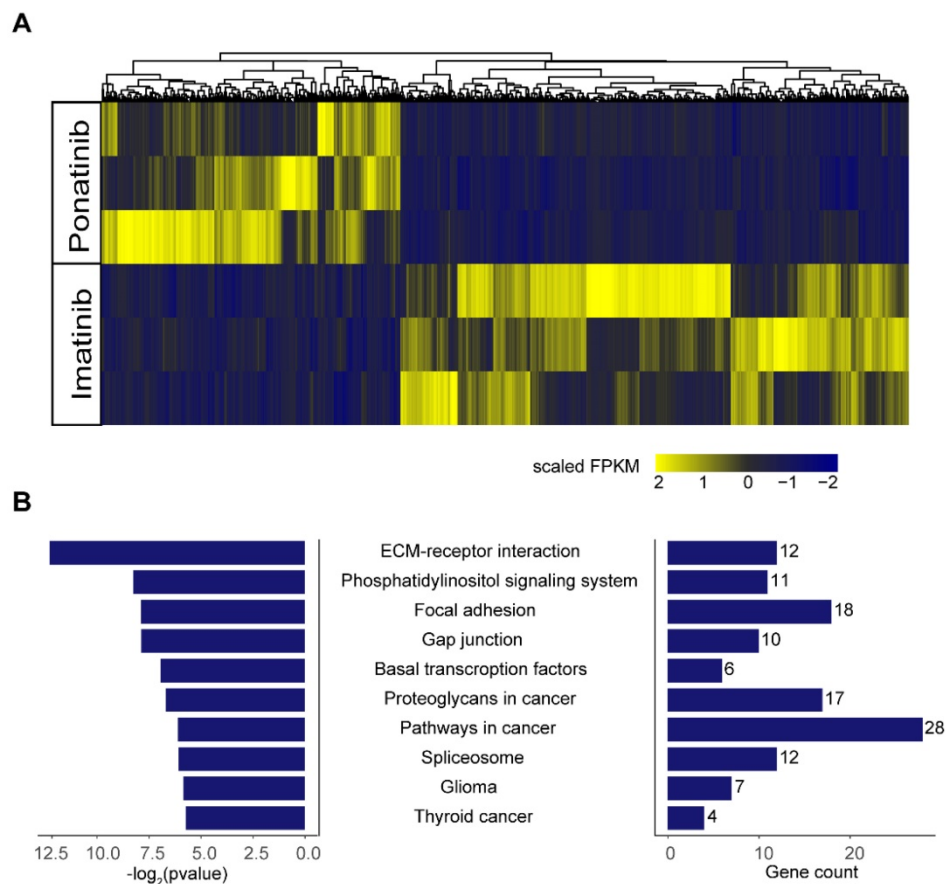


Figure 6. RNA-sequencing in tumors of PDX-KIT^{K642E} after 28 days of treatment with imatinib (n = 3) and ponatinib (n = 3). **(A)** Heatmap of differential expressed genes between the imatinib-treated group and ponatinib-treated group. **(B)** KEGG analysis showed that the ECM-receptor interaction pathway was the most significantly downregulated pathway in ponatinib-treated tumors compared with imatinib-treated tumors.

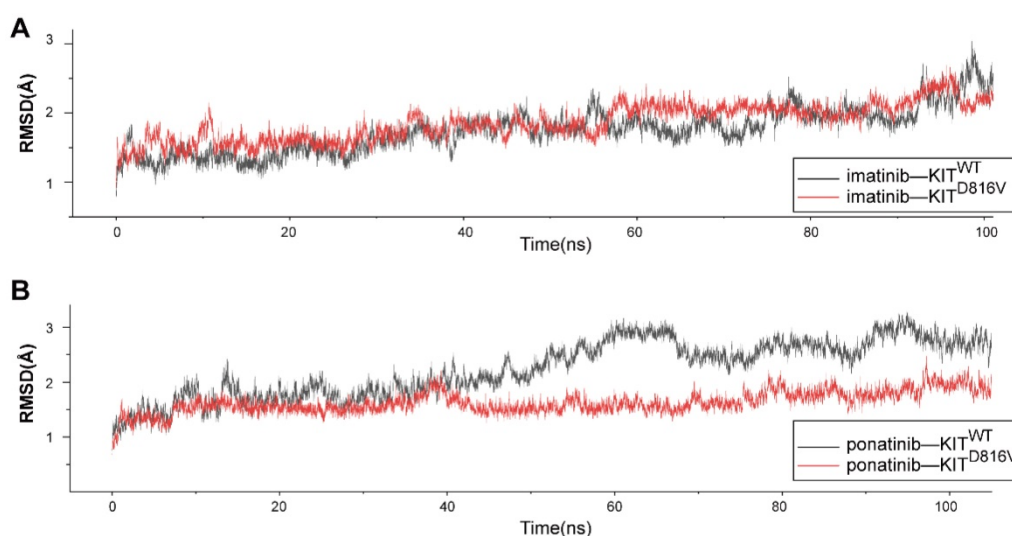


Figure 7. Molecular dynamic simulations of KIT^{WT}/KIT^{D816V} -ponatinib interactions. **(A)** RMSD of KIT^{WT}/KIT^{D816V} -imatinib complexes along 100 ns of MD simulations. **(B)** RMSD of KIT^{WT}/KIT^{D816V} -ponatinib complexes along 100 ns of MD simulations.

Discussion

This work successfully established a series of melanoma PDX models and PDCs with *KIT* mutations and used them for drug efficacy evaluations. Although the *in vitro* drug assays indicated that ponatinib was not the most effective inhibitor in all PDCs, except in the PDC- KIT^{D816V} , ponatinib induced the greatest growth inhibition efficacy against KIT^{D816V} -bearing PDX models compared with the other *KIT* inhibitors that were tested. Ponatinib is an FDA-approved kinase inhibitor for T315I-positive CML and Ph+ ALL patients, known to inhibit the kinase activity of *KIT*, *FGFR*, and *RET* [23, 27]. Previous studies have demonstrated the growth inhibitory efficacy of ponatinib in Ba-F3 cells with KIT^{V560D} or KIT^{K642E} mutations [23, 28]. Two additional studies indicated that ponatinib exerts growth inhibition and induces apoptosis in neoplastic mast cell lines harboring the KIT^{D816V} mutation [24]. However, no study has reported the use of ponatinib in melanoma. Our study thus demonstrated an unexpected opportunity to potentially repurpose ponatinib for use as a potent inhibitor for the treatment of *KIT*-mutant-bearing melanomas.

Mutations in the cancer driver gene *KIT* strongly affect the individual responses of patients to targeted therapies. In this vein of work, our study further complicates our knowledge of the interaction of imatinib with melanomas bearing *KIT* mutations: our finding that the PDX models with the KIT^{V560D} or KIT^{K642E} mutations did not respond to imatinib treatment does not align with the previously reported findings that melanomas with these mutations are sensitive to treatment with imatinib [8-10]. Thus, the prior conclusion that melanomas with KIT^{V560D} or

KIT^{K642E} mutations should be considered imatinib-sensitive will need to be examined in future work.

As more evidence accumulates about the *KIT*-mutation-related limits of the clinical benefits of imatinib as a treatment for melanomas, there have been multiple studies examining the use of other kinase inhibitor drugs. For example, dasatinib has shown potent preclinical activity against cells with KIT^{L576P} or KIT^{D820Y} mutation [29]. However, a phase II clinical trial of dasatinib in locally advanced or stage IV mucosal or acral melanoma patients showed a low response rate of among *KIT*-mutant or -amplified patients [12]. A notably different result from our findings in the present study, which showed strong TGI effects from dasatinib treatment for all three of the *KIT* mutation PDX models (Figure 4). Nilotinib can achieve disease control in patients with melanoma-harboring *KIT* alterations whose disease progressed after imatinib therapy [13]. For the other alternative kinase inhibitors that we tested in this study, the reported responses of melanomas to sunitinib were found to be unrelated to a *KIT* mutation, and no prolonged responses were observed compared to the response to imatinib. There is almost no *KIT* mutation-related information for sorafenib, but one patient with a *KIT* mutation-bearing melanoma was reported to respond well [30]. In addition, there is no study evaluating axitinib for the treatment of *KIT*-mutated tumor. Some other targeted strategies are also under investigation in *KIT*-driven melanoma. For example, SEL201, a MNK1/2 inhibitor was reported to suppress clonogenicity, cell migration, and *in vivo* tumor metastasis in KIT^{L576P} and KIT^{D820Y} mutant melanoma [29]; the translation of *KIT* is regulated by *LMTK3* in *KIT*-mutant gastrointestinal stromal tumor (GIST) and melanoma

while *LMTK3* silencing using a siRNA could reduce the viability of *KIT*-mutant cancer cells [31].

The application of MD simulations has been increasing in the field of protein kinase drug discovery; these simulations enable mechanistic investigations of biological and chemical events at an atomic level. Multiple MD studies have focused on *KIT* mutations. Additionally, electrostatic interactions play a significant role in the binding affinity of imatinib to *KIT* [32], and reduced electrostatic interactions may be responsible for the imatinib resistance to *KIT*^{D816V} [26], which is in accord with our simulation results that imatinib has a relatively lower binding affinity for *KIT*^{D816V} than does ponatinib. Consistently, our experiments with PDCs revealed that ponatinib treatment decreased the phosphorylation of both *KIT* and its downstream signaling targets, and RNA-seq analysis revealed that ponatinib significantly downregulated the ECM-receptor interaction pathway, which functions in the metastasis, proliferation, and apoptosis of tumor cell [33]. Thus, these data indicated that downregulation of the ECM-receptor interaction pathway was a potential mechanism mediating the robust efficacy of ponatinib in tumor growth inhibition when compared with imatinib. Looking forward, further investigation of ponatinib's molecular mechanisms, in concert with clinical studies about precisely which melanoma patient groups can benefit from ponatinib treatment, will help to further characterize the scientific basis and medicinal impact of the particularly strong efficacy that we observed for ponatinib drug in treating melanomas with *KIT* mutations.

Materials and Methods

Reagents

Axitinib, imatinib, dasatinib, ponatinib, sorafenib, sunitinib, and nilotinib were purchased from Selleck Chemical Inc (Houston, TX, USA). The following commercially available antibodies were purchased from Cell Signaling Technology (Danvers, MA, USA): *KIT* (#3074), phospho-*KIT* (Tyr719, #3391), *AKT* (#4685), phospho-*AKT* (Ser474, #4060), *ERK1/2* (#4695), phospho-*ERK1/2* (Tyr202/Tyr204, #4370), and *GAPDH* (#2118). Rabbit polyclonal antibody against human Ki67 (ab15580) was purchased from Abcam (Cambridge, UK). Rabbit polyclonal antibody against human S-100A (catalog, GZ031129), mouse polyclonal antibodies against human Melan-A (catalog, GM719629) and HMB-45 (catalog, GM063429) were purchased from GeneTech company limited (shanghai, China). Terminal deoxynucleotidyl transferase dUTP nick-end labeling (TUNEL) *KIT* and CCK-8 *KIT* were purchased from Bimake (Houston,

TX, USA).

Establishment of *KIT* mutant patient-derived tumor xenografts from melanomas

Fresh tumor samples from melanoma patients were collected following informed consent for engraftment in accordance with the ethical guidelines approved for this study by the Institutional Review and the Ethics Committee of Shanghai Ninth People's Hospital, Shanghai Jiao Tong University School of Medicine. Mice were maintained and all procedures were performed under the approval and supervision of the Institutional Animal Care and Use Committee (IACUC) of Shanghai Jiao Tong University School of Medicine.

Before engraftment, necrotic tissues were carefully removed from the tumor samples using a sterilized scalpel. Approximately 3×3×3-mm³ tissue fragments were implanted subcutaneously into the flank region of nude or NOD-SCID mice (male, 5-6 weeks old). Successfully engrafted tumor models were then passaged and banked using standard methods. The passage directly harboring the patient samples was termed P0; subsequent generations were consecutively named P1, P2, P3, P4, etc. After each passage, harvested tumor samples were divided into several segments for subsequent implantation, for cryopreservation in liquid nitrogen and freezing media, and for histopathological analysis in paraffin embedding.

Generation of patient-derived tumor cells

Tumor tissues from the *KIT* mutant PDXs were extensively washed with serum-free RPMI1640 (Gibco, Waltham, MA, USA) and minced using a sterile scalpel and dissociated in RPMI1640 with 1 mg/ml IV collagenase (Sigma-Aldrich, St. Louis, MO, USA) and 0.5 mg/mL dispase (Gibco) for 2h at 37°C with agitation. Cells were filtered through a 40-μm filter and washed twice in PBS and suspended in RPMI 1640 medium with 10% fetal bovine serum (Gibco) and 1% penicillin and streptomycin. Cells were cultured at 37°C in a humidified atmosphere of 95% air and 5% CO₂.

TUNEL assay

The incidence of apoptotic tumor cells was assessed by terminal deoxynucleotidyl transferase-mediated dUTP nick end labeling (TUNEL) staining. TUNEL staining was performed according to the manufacturer's protocols. The slides were deparaffinized in xylene and hydrated in graded ethanol. Then, sections were washed with PBS and incubated with proteinase K for 20 min at 37°C. After washing three times with PBS, the sections were treated with 50 μl of TUNEL reaction mix and then

washed three times. Nuclei were counterstained with 4, 6-diamidino-2-phenylindole (DAPI) at 37°C for 10 minutes.

Immunofluorescence staining

For tissue sections, after deparaffinization, sections were hydrated and underwent sodium citrate antigen retrieval and then incubated with 3% hydrogen peroxide to block endogenous peroxidase activity. For PDCs, the cells were grown on glass coverslips, washed with PBS, fixed with 4% paraformaldehyde in PBS for 15 minutes, permeabilized with 0.5% Triton X-100 for 10 minutes, and blocked with 5% goat serum in PBS at 37°C for 30 minutes. Sections or cells were incubated with primary antibodies against Ki67 (1:200 dilution), Melan-A (1:100 dilution), and HMB-45 (1:100 dilution) overnight at 4°C, followed by Alexa Fluor 488-conjugated AffiniPure goat anti-mouse IgG (H+L) or Alexa Fluor 594-conjugated goat anti-rabbit IgG (H+L) second antibodies for 60 minutes. Nuclei were counterstained with 4, 6-diamidino-2-phenylindole (DAPI) at 37°C for 10 minutes. In the negative control samples, the primary antibody was replaced with PBS.

Cell viability assay

Cell viability was determined using a cell counting kit-8 (CCK-8) assay. Cells were seeded into 96-well plates at a density of 2,000 cells per well and treated with vehicle (DMSO) control or inhibitors with serial dilution for 72 h. The IC₅₀ values were calculated using GraphPad Prism software.

Generation of Ba-F3 stable cell lines

Full-length cDNAs of *KIT* containing *KIT*^{WT}, *KIT*^{V560D}, *KIT*^{K642E} and *KIT*^{D816V} were generated by mutagenesis and were cloned into the pLVX-IRES-Puro vector according to the manufacturer's instructions. Ba-F3 cells expressing *KIT*^{WT}, *KIT*^{V560D}, *KIT*^{K642E} and *KIT*^{D816V} mutation constructs were selected in RPMI 1640 supplemented with SCF (20 ng/ml) and puromycin (1 μg/ml). These cells were maintained until IL-3-independent cells emerged. Parental Ba/F3 cells, as a control, were cultured in RPMI 1640 media supplemented with IL-3.

In vivo drug efficacy evaluation

PDX mice were randomized into treatment groups when the average tumor volume reached ~250 mm³. Treatment compounds were administered to mice daily by oral gavage as follows: water and citrate (25 mM, pH=2.75), imatinib mesylate (100 mg/kg, diluted in water), dasatinib (30 mg/kg), and ponatinib (30 mg/kg). Both dasatinib and ponatinib were diluted in citrate buffer (25 mM, pH=2.75). Tumor size was measured with calipers, and mouse weight was

recorded twice weekly. Tumor volume (mm³) was calculated as follows: tumor volume = $L \times W^2 \times 0.5$, where L represents the largest diameter and W represents the minor tumor axis. When the treatment was terminated, tumor growth inhibition (TGI) was calculated as follows: $TGI = 1 - [(TV_{f,treated} - TV_{i,treated}) / (TV_{f,control} - TV_{i,control})] \times 100\%$, where TV_f is the average tumor volume at the end of the experiment, and TV_i is the average tumor volume at the start of treatment.

Immunoblotting

Immunoblotting was performed using standard SDS-PAGE protocols. Briefly, the proteins were separated on SDS-PAGE gels and transferred to PVDF membranes. The membrane was incubated with primary antibodies against *KIT* (dilution 1:1000), phospho-*KIT* (dilution 1:1000), AKT (dilution 1:1000), phospho-AKT (dilution 1:1000), ERK1/2 (dilution 1:1000), phospho-ERK1/2 (dilution 1:2000), or GAPDH (dilution 1:1000) overnight at 4°C. After washing and incubation with secondary antibodies, signals were visualized using an Odyssey Infrared Imaging System (Biosciences) according to the product instructions.

RNA-Sequencing and analysis

RNA was isolated from snap-frozen tumors from vehicle-, imatinib-, and ponatinib-treated mice. Total RNA was extracted using RNeasy Mini Kit (Cat# 74106, Qiagen) following the manufacturer's instructions and checked for a RIN number to inspect RNA integrity by an Agilent Bioanalyzer 2100 (Agilent technologies, Santa Clara, CA, US). Qualified total RNA was further purified by RNAClean XP Kit (Cat A63987, Beckman Coulter, Inc. Kraemer Boulevard Brea, CA, USA) and RNase-Free DNase Set (Cat#792 54, QIAGEN, GmbH, Germany). The Illumina TruSeq RNA Sample Preparation Kit (Illumina) was used for library preparation. RNA sequencing were performed on the Illumina HiSeq 2000 platform. Reads were aligned with human transcript genome (hg38) using TopHat v2. Gene expression abundance was estimated by Stringtie (version: 1.3.0). Differentially expression analysis was determined using negative binomial model via EdgeR/DESeq2, by comparing imatinib-treated with ponatinib-treated tumors and *P*-value was calculated using Wald test, multiple test correction was performed using B-H procedure, with a fold change (FC) >2.0 and *P* < 0.05 as the cut-off criteria. Pathway analysis on differentially expressed genes was performed using KEGG pathway analysis.

Molecular dynamics simulations

The co-structure of *KIT*^{WT}-ponatinib (PDB ID: 4U0I) [23] and *KIT*^{WT}-imatinib (PDB ID: 1T46) [34] were retrieved from the PDB library. Pymol was

used for the *in silico* substitution of the Asp (D) to Val (V) KIT mutation at position 816. Molecular dynamics (MD) simulations of four complexes (KIT^{WT}-imatinib, KIT^{WT}-ponatinib, KIT^{D816V}-imatinib, and KIT^{D816V}-ponatinib) were performed using Amber (V14.0) with a previously reported approach [35]. Briefly, the energy of the systems was minimized, relaxed and then heated to reach equilibration. The four complexes underwent 100-ns MD simulations in isothermal and isobaric conditions. The trajectories were recorded every 20 ps. The root-mean-square deviation (RMSD) of the trajectories was calculated to present the dynamic conformational changes throughout the MD simulations. Superposition of structural conformations was taken at 100 ns from the MD simulations. The binding free energy (ΔG binding) of KIT^{D816V}-ponatinib was calculated using Molecular Mechanics Generalized Born Surface Area (MM-GBSA) analysis. The electrostatic potential surface was computed with the APBS software through the PDB2PQR webserver (<http://nbcrc-222.ucsd.edu/pdb2pqr/>). The conformations of the KIT^{D816V}-imatinib and KIT^{D816V}-ponatinib complexes after 100 ns MD simulations were used as input data. Plots were generated using APBS tools plugin available with Pymol software[36].

Statistics

Analyses were conducted with GraphPad Prism version 6.0 for Windows (GraphPad Software, La Jolla, CA, USA). The results are represented as the mean \pm SEM of at least three replicate samples for each group, unless noted otherwise. Unpaired Student's *t*-tests were performed to compare differences between the two groups. *P* < 0.05 was considered statistically significant.

Abbreviations

ECM: Extracellular matrix; FC: Fold change; IC₅₀: half maximal inhibitory concentration; KEGG: Kyoto Encyclopedia of Genes and Genomes; NCCN: National Comprehensive Cancer Network; MD: molecular dynamics; PDX: patient-derived tumor xenograft; PDC: PDX-derived tumor cells; TGI: tumor growth inhibition.

Acknowledgements

The authors thank Professor Qiancheng Shen, Department of Pathophysiology, Key Laboratory of Cell Differentiation and Apoptosis of Ministry of Education, Shanghai Jiao Tong University School of Medicine, for helpful direction regarding the MD simulations.

Funding

This work was funded by The National Key Research and Development Program of China (2017YFC0908500) and also funded by grants from the National Natural Science Foundation of China (81572656, 8187219, 81202131).

Supplementary Material

Supplementary figures and tables.

<http://www.thno.org/v09p1952s1.pdf>

Competing Interests

The authors have declared that no competing interest exists.

References

- Ossio R, Roldán-Marín R, Martínez-Said H, Adams DJ, Robles-Espinoza CD. Melanoma: a global perspective. *Nat Rev Cancer*. 2017; 17: 393.
- Genomic Classification of Cutaneous Melanoma. *Cell*. 2015; 161: 1681-96.
- McArthur GA, Chapman PB, Robert C, Larkin J, Haanen JB, Dummer R, et al. Safety and efficacy of vemurafenib in BRAF(V600E) and BRAF(V600K) mutation-positive melanoma (BRIM-3): extended follow-up of a phase 3, randomised, open-label study. *Lancet Oncol*. 2014; 15: 323-32.
- Curtin JA, Busam K, Pinkel D, Bastian BC. Somatic activation of KIT in distinct subtypes of melanoma. *J Clin Oncol*. 2006; 24: 4340-6.
- Todd JR, Scurr LL, Becker TM, Kefferd RF, Rizos H. The MAPK pathway functions as a redundant survival signal that reinforces the PI3K cascade in c-Kit mutant melanoma. *Oncogene*. 2014; 33: 236-45.
- Heinrich MC, Griffith DJ, Druker BJ, Wait CL, Ott KA, Ziegler AJ. Inhibition of c-kit receptor tyrosine kinase activity by STI 571, a selective tyrosine kinase inhibitor. *Blood*. 2000; 96: 925-32.
- Carvajal RD. Another option in our KIT of effective therapies for advanced melanoma. *J Clin Oncol*. 2013; 31: 3173-5.
- Hodi FS, Corless CL, Giobbie-Hurder A, Fletcher JA, Zhu M, Marino-Enriquez A, et al. Imatinib for melanomas harboring mutationally activated or amplified KIT arising on mucosal, acral, and chronically sun-damaged skin. *J Clin Oncol*. 2013; 31: 3182-90.
- Carvajal RD, Antonescu CR, Wolchok JD, Chapman PB, Roman RA, Teitcher J, et al. KIT as a therapeutic target in metastatic melanoma. *JAMA*. 2011; 305: 2327-34.
- Guo J, Si L, Kong Y, Flaherty KT, Xu X, Zhu Y, et al. Phase II, open-label, single-arm trial of imatinib mesylate in patients with metastatic melanoma harboring c-Kit mutation or amplification. *J Clin Oncol*. 2011; 29: 2904-9.
- Minor DR, Kashani-Sabet M, Garrido M, O'Day SJ, Hamid O, Bastian BC. Sunitinib therapy for melanoma patients with KIT mutations. *Clin Cancer Res*. 2012; 18: 1457-63.
- Kalinsky K, Lee S, Rubin KM, Lawrence DP, Iafrate AJ, Borger DR, et al. A phase 2 trial of dasatinib in patients with locally advanced or stage IV mucosal, acral, or vulvovaginal melanoma: A trial of the ECOG-ACRIN Cancer Research Group (E2607). *Cancer*. 2017; 123: 2688-97.
- Guo J, Carvajal RD, Dummer R, Hauschild A, Daud A, Bastian BC, et al. Efficacy and safety of nilotinib in patients with KIT-mutated metastatic or inoperable melanoma: final results from the global, single-arm, phase II TEAM trial. *Ann Oncol*. 2017; 28: 1380-7.
- Yun J, Lee J, Jang J, Lee EJ, Jang KT, Kim JH, et al. KIT amplification and gene mutations in acral/mucosal melanoma in Korea. *APMIS*. 2011; 119: 330-5.
- Hintzsche JD, Gorden NT, Amato CM, Kim J, Wuensch KE, Robinson SE, et al. Whole-exome sequencing identifies recurrent SF3B1 R625 mutation and comutation of NF1 and KIT in mucosal melanoma. *Melanoma Res*. 2017; 27: 189-99.
- Kong Y, Si L, Zhu Y, Xu X, Corless CL, Flaherty KT, et al. Large-scale analysis of KIT aberrations in Chinese patients with melanoma. *Clin Cancer Res*. 2011; 17: 1684-91.
- Bruna A, Rueda OM, Greenwood W, Batra AS, Callari M, Batra RN, et al. A Biobank of Breast Cancer Explants with Preserved Intra-tumor Heterogeneity to Screen Anticancer Compounds. *Cell*. 2016; 167: 260-74.e22.
- Izumchenko E, Paz K, Ciznadija D, Sloma I, Katz A, Vasquez-Dunddel D, et al. Patient-derived xenografts effectively capture responses to oncology therapy in a heterogeneous cohort of patients with solid tumors. *Ann Oncol*. 2017; 28: 2595-605.
- Hidalgo M, Amant F, Biankin AV, Budinska E, Byrne AT, Caldas C, et al. Patient-derived xenograft models: an emerging platform for translational cancer research. *Cancer Discov*. 2014; 4: 998-1013.
- Aparicio S, Hidalgo M, Kung AL. Examining the utility of patient-derived xenograft mouse models. *Nat Rev Cancer*. 2015; 15: 311-6.

21. Phung B, Kazi JU, Lundby A, Bergsteinsdottir K, Sun J, Goding CR, et al. KIT(D816V) Induces SRC-Mediated Tyrosine Phosphorylation of MITF and Altered Transcription Program in Melanoma. *Mol Cancer Res.* 2017; 15: 1265-74.
22. Mol CD, Lim KB, Sridhar V, Zou H, Chien EY, Sang BC, et al. Structure of a c-kit product complex reveals the basis for kinase transactivation. *J Biol Chem.* 2003; 278: 31461-4.
23. Garner AP, Gozgit JM, Anjum R, Vodala S, Schrock A, Zhou T, et al. Ponatinib inhibits polyclonal drug-resistant KIT oncoproteins and shows therapeutic potential in heavily pretreated gastrointestinal stromal tumor (GIST) patients. *Clin Cancer Res.* 2014; 20: 5745-55.
24. Jin B, Ding K, Pan J. Ponatinib induces apoptosis in imatinib-resistant human mast cells by dephosphorylating mutant D816V KIT and silencing beta-catenin signaling. *Mol Cancer Ther.* 2014; 13: 1217-30.
25. Heinrich MC, Corless CL, Demetri GD, Blanke CD, von Mehren M, Joensuu H, et al. Kinase mutations and imatinib response in patients with metastatic gastrointestinal stromal tumor. *J Clin Oncol.* 2003; 21: 4342-9.
26. Da Silva Figueiredo Celestino Gomes P, Chauvot De Beauchene I, Panel N, Lopez S, De Sepulveda P, Geraldo Pascutti P, et al. Insight on Mutation-Induced Resistance from Molecular Dynamics Simulations of the Native and Mutated CSF-1R and KIT. *PloS one.* 2016; 11: e0160165.
27. O'Hare T, Shakespeare WC, Zhu X, Eide CA, Rivera VM, Wang F, et al. AP24534, a pan-BCR-ABL inhibitor for chronic myeloid leukemia, potently inhibits the T315I mutant and overcomes mutation-based resistance. *Cancer Cell.* 2009; 16: 401-12.
28. Lierman E, Smits S, Cools J, Dewaele B, Debiec-Rychter M, Vandenberghe P. Ponatinib is active against imatinib-resistant mutants of FIP1L1-PDGFR α and KIT, and against FGFR1-derived fusion kinases. *Leukemia.* 2012; 26: 1693-5.
29. Zhan Y, Guo J, Yang W, Goncalves C, Rzymiski T, Dreas A, et al. MNK1/2 inhibition limits oncogenicity and metastasis of KIT-mutant melanoma. *J Clin Invest.* 2017; 127: 4179-92.
30. Quintas-Cardama A, Lazar AJ, Woodman SE, Kim K, Ross M, Hwu P. Complete response of stage IV anal mucosal melanoma expressing KIT Val560Asp to the multikinase inhibitor sorafenib. *Nat Clin Pract Oncol.* 2008; 5: 737-40.
31. Klug LR, Bannon AE, Javidi-Sharifi N, Town A, Fleming WH, VanSlyke JK, et al. LMTK3 is essential for oncogenic KIT expression in KIT-mutant GIST and melanoma. *Oncogene.* 2018.
32. Lin YL, Roux B. Computational analysis of the binding specificity of Gleevec to Abl, c-Kit, Lck, and c-Src tyrosine kinases. *J Am Chem Soc.* 2013; 135: 14741-53.
33. Gilkes DM, Semenza GL, Wirtz D. Hypoxia and the extracellular matrix: drivers of tumour metastasis. *Nat Rev Cancer.* 2014; 14: 430-9.
34. Mol CD, Dougan DR, Schneider TR, Skene RJ, Kraus ML, Scheibe DN, et al. Structural basis for the autoinhibition and STI-571 inhibition of c-Kit tyrosine kinase. *J Biol Chem.* 2004; 279: 31655-63.
35. Case DA, Cheatham TE, 3rd, Darden T, Gohlke H, Luo R, Merz KM, Jr., et al. The Amber biomolecular simulation programs. *J Comput Chem.* 2005; 26: 1668-88.
36. Dolinsky TJ, Nielsen JE, McCammon JA, Baker NA. PDB2PQR: an automated pipeline for the setup of Poisson-Boltzmann electrostatics calculations. *Nucleic Acids Res.* 2004; 32: W665-7.